Hindawi
Advances in High Energy Physics
Volume 2021, Article ID 5519028, 12 pages
https://doi.org/10.1155/2021/5519028

*Research Article*

# Cosmic Consequences of Kaniadakis and Generalized Tsallis Holographic Dark Energy Models in the Fractal Universe

**Abdul Jawad**[1] **and Abdul Malik Sultan**[1,2]

[1]*Department of Mathematics, COMSATS University Islamabad, Lahore Campus 54000, Pakistan*
[2]*Department of Mathematics, University of Okara, Okara 56130, Pakistan*

Correspondence should be addressed to Abdul Jawad; jawadab181@yahoo.com

Received 2 February 2021; Revised 24 March 2021; Accepted 3 April 2021; Published 20 April 2021

Academic Editor: Hooman Moradpour



We investigate the recently proposed holographic dark energy models with the apparent horizon as the IR cutoff by assuming Kaniadakis and generalized Tsallis entropies in the fractal universe. The implications of these models are discussed for both the interacting ($\Gamma = 3Hb^2\rho_m$) and noninteracting ($b^2 = 0$) cases through different cosmological parameters. Accelerated expansion of the universe is justified for both models through deceleration parameter $q$. In this way, the equation of state parameter $\omega_d$ describes the phantom and quintessence phases of the universe. However, the coincidence parameter $\tilde{r} = \Omega_m/\Omega_d$ shows the dark energy- and dark matter-dominated eras for different values of parameters. It is also mentioned here that the squared speed of sound gives the stability of the model except for the interacting case of the generalized Tsallis holographic dark energy model. It is mentioned here that the current dark energy models at the apparent horizon give consistent results with recent observations.

## 1. Introduction

To acquire a unified understanding of various entropy measures and how they connect to each other in a generalized form, it is required to recall characteristics of "classical" entropies. In information theory, information can be collected through the probability distribution of some events that belong to the sample space of all possible events which are called entropies. Gibbs was the first who stated a hypothesis [1] which was the source of inspiration for people to define numerous entropies [2–4]. We hear and read frequently as it is claimed due to Gibbs that the black hole (BH) entropy is proportional to the area of the BH boundary in spite of having proportionality to the volume of BH. In recent times, these entropies have been the source for the modeling of cosmic evolution in different setups [5–7]. It is a matter of fact that to retrieve thermodynamical extensivity for nonstandard systems, the entropies generalizing that of Boltzman-Gibbs (BG) become necessary. For the study of BH, generalized entropies have been employed [8–11], also for the construction of new holographic dark energy (HDE) models [12, 13]. Besides this, it has been revealed that such kind of entropies can affect the Jeans mass [14], can provide a theoretical basis for the modified Newtonian dynamics (MOND) theory [15], may be inspired by the quantum features of gravity [16], and even may illustrate inflation without assuming inflation [17]. The foundation stone of primary HDE [18] is a holographic principle, and it is proposed on Bakenstein entropy [19–21]. It is observed that the Hubble horizon is a proper casual boundary for the universe meeting thermodynamics and conservation laws [22–25]. However, HDE suffers from some problems when the Hubble horizon is considered the IR cutoff [18, 26]. Some other HDE models based on generalized entropy can give a considerable description of accelerated expansion of the universe even when the apparent horizon is used as the IR cutoff [12, 13, 27]. Consequently, more suitable models of HDE may be found using generalized entropies.

The Tsallis entropy is a generalized form of BG entropy which was presented in 1988 by Constantino Tsallis [28] as

a fundamental to generalize the standard statistical mechanics. In the literature, there is a wide debate regarding the physical relevance of Tsallis entropy [29, 30]. However, at the start of the 21st century, there is an identified increasing wide spectrum of an artificial, natural, and social complex system which certifies the consequences and predictions that resulted from this nonadditive entropy (i.e., nonextensive statistical mechanics). In this regard, one of the most precise investigated frameworks is developed by Kaniadakis which is the Tsallis nonextensive statistical mechanics and the generalized power law statistics [28].

A lot of work has been done by Dubey et al. [31], Sharma et al. [32–34], Srivastava et al. [35], and Ghaffari et al. [17, 36] on cosmic expansion in various theories of gravity by using recently obtained DE models such as new Tsallis HDE (NTHDE), Réyni HDE (RHDE), and Barrow HDE (BHDE). They have made versatile studies on accelerated expansion of the universe through various cosmological parameters and planes and found consistent results with recent Planck's data [37]. In recent times, the Kaniadakis statistics have been studied as generalized entropy measures [2, 4] with some gravitational and cosmological consequences [7, 38]. In view of these generalized entropies, HDE models have been developed by Moradpour et al. [11]. They have examined the deceleration parameter, EoS parameter, and coincidence parameter for these models and found consistent results with recent Planck's data. It is suggested that generalized entropies must obey fundamental laws of thermodynamics such as the zeroth law [39–43]. The above arguments and work done are the sources of motivation due to which we are going to examine BH entropy in the different well-known generalized entropy formalisms and study their capability in representing the current accelerated expansion of the universe by formulating their corresponding HDE models.

In the next section, Tsallis entropy of BH will be calculated using the relation of Boltzmann and Tsallis entropies. Additionally, Kaniadakis entropy of BH will be computed using the relationship of Kaniadakis statistics with Tsallis entropy. Moreover, Sharma-Mittal and Rényi entropies of BH will also be discussed by applying their relation with Tsallis entropy. In Section 3, the Kaniadakis holographic dark energy (KHDE) will be discussed along with some of its cosmological consequences such as deceleration parameter $q$, EoS parameter $\omega_d^K$, and the dimensionless ratio called coincidence parameter $\tilde{r} = \Omega_m/\Omega_d^K$ for both the interacting and noninteracting cases. The stability of the achieved model for both the interacting and noninteracting cases is also analyzed by the squared speed of sound $C_s^2$. In Section 4, the NTHDE of BH will be discussed. We will find some cosmological parameters using this model for both the noninteracting and interacting cases such as deceleration parameter $q$, EoS parameter $\omega_d^T$, and the dimensionless ratio called coincidence parameter $\tilde{r} = \Omega_m/\Omega_d^T$. The squared speed of sound $C_s^2$ will also be evaluated to investigate the stability of the model taking both the interacting and noninteracting cases into account. In Section 5, achieved results are compared with the observational data and some concluding remarks about our work have been discussed.

## 2. Tsallis and Kaniadakis Entropies of BH

Both the Gibbs [1] and Shannon [44] entropies of distribution with $W$ states working in the unit $k_B = 1$ leads to the relation explicitly dealt in [11]:

$$S = -\sum_{i=1}^{W} P_i \ln (P_i), \tag{1}$$

where $P_i$ represents the probability of occupying the $i$th state for the classical system. The so-called von Neumann entropy which is a quantum mechanical form of this entropy is represented as

$$S = -Tr[\rho \ln (\rho)]. \tag{2}$$

The utilization of Equation (2) for the classical system goes back to the proposal of Boltzmann, where $\rho$ represents the state density in the phase space [45]. One can obtain the so-called Bekenstein entropy ($S_{\mathrm{BH}} = A/4$) by applying Equation (2) to a purely gravitational system [19]. Since degrees of freedom are disseminated on the horizon without any preference w.r.t. one another, one may consider that $P_i$ is equal for all of them [20, 21] permitting us to write $P_i = 1/W$. In such manner, Equations (1) and (2) lead to the Boltzmann entropy ($S = \ln (W)$), and thus, we have [7]

$$S_{\mathrm{BH}} = \frac{A}{4} = \ln (W) \Rightarrow W = \exp\left(\frac{A}{4}\right), \tag{3}$$

for horizon entropy and accordingly $W(A)$. As a unique free parameter generalized entropy, the Tsallis entropy is defined as [4]

$$S_Q^T = \frac{1}{1-Q}\sum_{i=1}^{W}\left(P_i^Q - P_i\right), \tag{4}$$

where $Q$ is an unknown free parameter named as the nonextensive or Tsallis parameter ($S_Q^T \to S$ for $Q \to 1$). When the probability distribution meets the conditions $P_i = 1/W$, Equation (4) yields

$$S_Q^T = \frac{W^{1-Q} - 1}{1-Q}. \tag{5}$$

The quantum features of gravity [7, 46] are also a source for the existence of $Q$ parameter. Now, taking $\delta = 1 - Q$ and utilizing Equation (3) with Equation (5), one can find easily

$$S_Q^T = \frac{1}{1-Q}\left[\exp\left((1-Q)S_{\mathrm{BH}}\right) - 1\right] = \frac{2\exp\left(\delta S_{\mathrm{BH}}/2\right)}{\delta}\sinh\left(\frac{\delta S_{\mathrm{BH}}}{2}\right). \tag{6}$$

In the scenario of loop quantum gravity, it is acquired by applying the Tsallis entropy definition to BH [11, 47] that

$$S_Q^T = \frac{1}{1-Q}\left[\exp\left(\frac{(1-Q)\ln(2)}{\pi\beta\sqrt{3}}S_{\mathrm{BH}}\right)-1\right], \quad (7)$$

satisfying $S_Q^T \to S$ whenever $Q \to 1$ and $\beta = \ln(2)/\pi\sqrt{3}$ [11, 47]. Furthermore, Equation (6) and (7) become accordingly the same when we consider $\beta = \ln(2)/\pi\sqrt{3}$.

Another single-free parameter generalized entropy is Kaniadakis entropy ($K$-entropy) [2, 3, 11], defined as

$$S_K = -\sum_{i=1}^{W}\frac{P_i^{1+K}-P_i^{1-K}}{2K} = \frac{1}{2}\left(\frac{\Sigma_{i=1}^{W}\left(P_i^{1-K}-P_i\right)}{K}+\frac{\Sigma_{i=1}^{W}\left(P_i^{1+K}-P_i\right)}{-K}\right), \quad (8)$$

where $K$ represents an unknown parameter, and the limit $K \to 0$ is a way to obtain Boltzmann-Gibbs entropy [2, 3]. Comparing Equation (8) with (4) and (5), it can easily obtain

$$S_K = \frac{S_{1+K}^T + S_{1-K}^T}{2}. \quad (9)$$

Furthermore, by taking $P_i = 1/W$, Equation (8) assists in getting [2, 3, 11]

$$S_K = \frac{W^K - W^{-K}}{2K}. \quad (10)$$

Combining Equation (10) with Equation (3) yields

$$S_K = \frac{1}{K}\sinh(KS_{\mathrm{BH}}). \quad (11)$$

It is observed that Sharma-Mittal and Rényi entropies can be obtained as a function of Tsallis entropy as [13, 48]

$$S_{\mathrm{SM}} = \frac{1}{R}\left(\left(1+(1-Q)S_T\right)^{R/1-Q}-1\right), \qquad \mathcal{S} = \frac{1}{1-Q}\ln\left(1+(1-Q)S_T\right), \quad (12)$$

which leads to

$$S_{\mathrm{SM}} = \frac{1}{R}\left[\exp(RS_{\mathrm{BH}})-1\right], \quad \mathcal{S} = S_{\mathrm{BH}}, \quad (13)$$

where $R$ is an unknown parameter. It is suggested that $\beta = \ln(2)/\pi\sqrt{3}$; otherwise, $(\ln(2)/\beta\pi\sqrt{3})S_{\mathrm{BH}}$ would occur in mathematical results rather than $S_{\mathrm{BH}}$.

## 3. Kaniadakis Holographic Dark Energy

As it was claimed by the HDE hypothesis that if the current accelerated universe is driven by vacuum energy, then its total amount stored in a packet with size $L^3$ should not go beyond the energy of BH having the same size as it [18]. By keeping in mind this, one can generate the following relation in view of Kaniadakis entropy (11) as

$$\Lambda^4 = \rho_d^K \propto \frac{S_K}{L^4}, \quad (14)$$

for the vacuum energy $\rho_d^K$. Now, taking the Hubble horizon of the cosmos as the IR cutoff (i.e., $L = 1/H \Rightarrow A = 4\pi/H^2$), we obtain

$$\rho_d^K = \frac{3c^2H^4}{8\pi\kappa}\sinh\left(\frac{\pi\kappa}{H^2}\right), \quad (15)$$

where the constant $c^2$ is unknown [18], $\kappa$ belongs to a set of real numbers [3], and $H = \dot{a}/a$ is the Hubble parameter. Now, it is clear that we have $\rho_d^K \to 3c^2H^2/8$ (the well-known Bekenstein entropy-based HDE) when $k \to 0$ [18]. Considering the pressureless fluid (with energy density $\rho_m$) and the dark energy candidate (with pressure $p_d$ and density $\rho_d^K$), the energy-momentum conservation laws for the fractal universe take the form

$$\dot{\rho}_m + \left(3H + \frac{\dot{\upsilon}}{\upsilon}\right)\rho_m = \Gamma, \quad (16)$$

$$\dot{\rho}_d + \left(3H + \frac{\dot{\upsilon}}{\upsilon}\right)(\rho_d + p_d) = -\Gamma, \quad (17)$$

where the "dot" represents the derivative w.r.t. cosmic time $t$, and the phenomenal term $\Gamma$ represents the interaction between dark matter and DE (it also gives the flow of energy between the two fluids) and has different mathematical values for both the linear and nonlinear cases, among which some linear cases are $\Gamma_1 = 3Hb^2(\rho_m + \rho_d)$, $\Gamma_2 = 3Hb^2\rho_m$, and $\Gamma_3 = 3Hb^2\rho_d$ [49–54] while some nonlinear cases are $\Gamma_4 = 3Hb^2((\rho_m^2/(\rho_m+\rho_d)) + \rho_m)$, $\Gamma_5 = 3Hb^2((\rho_d^2/(\rho_m+\rho_d)) + \rho_d)$, $\Gamma_6 = 3Hb^2((\rho_d^2/(\rho_m+\rho_d)) + \rho_d + \rho_m)$, and $\Gamma_7 = 3Hb^2((\rho_m^2/(\rho_m+\rho_d)) + \rho_d + \rho_m)$ [53, 54] with $b^2$ being the coupling constant. We have chosen $\Gamma = 3Hb^2\rho_m$ [49] as it is simple and leads to precise results. The fractal profile is either timelike or spacelike. We have chosen the timelike fractal profile in the power law form as $\upsilon = a^{-\gamma}$ [36, 55] with $a$ being the scale factor depending upon cosmic time $t$ and $\gamma$ being a positive constant. In the fractal universe, the Friedmann equations can be obtained as

$$H^2 + H\frac{\dot{\upsilon}}{\upsilon} - \frac{\omega}{6}\dot{\upsilon}^2 = \frac{1}{3}(\rho_m + \rho_d), \quad (18)$$

$$\dot{H} + H^2 - H\frac{\dot{\upsilon}}{\upsilon} + \frac{\omega}{3}\upsilon^2 - \frac{\Box\upsilon}{2\upsilon} = -\frac{1}{6}(\rho + 3p), \quad (19)$$

where $\Box\upsilon = (1/\sqrt{-g})\partial^\mu(\sqrt{-g}\partial_\mu\upsilon)$ with simplified relation as $\Box\upsilon = -[\ddot{\upsilon} + 3H\dot{\upsilon}]$. From simplification of (16), one can find

$$\rho_m = \frac{3\Omega_{m_o}H_o^2}{8\pi}(1+z)^{\Delta}, \quad (20)$$

where $\Delta = 3 - \gamma - 3b^2$, $z$ represents the redshift parameter, $H_o$ is the value of the Hubble parameter at $t = 0$, and $\Omega_{m_o} = 8\pi\rho_{m_o}/3H_o^2$ with $\rho_{m_o}$ being a constant of integration.

The scope and importance of cosmological parameters is increasing day by day as they are favorable tools to analyze and track the history and evaluation of the universe. The parameter $q$ is one which decides whether the universe is facing accelerated expansion or not (i.e., $q < 0$ gives the accelerated expansion of the universe while $q > 0$ when the universe has decelerating expansion behavior) [56, 57]. The equation of state (EoS) parameter $\omega_d$ is one which decides the phases of the cosmos (i.e., $\omega_d < -1$ represents the phantom phase of the universe, and $-1 < \omega_d < -1/3$ describes the quintessence phase while $\omega_d > -1/3$ gives the vacuum phase of the universe) [58, 59]. The squared speed of sound $C_s^2$ is another important cosmological parameter which decides whether the model is stable or not (i.e., $C_s^2 > 0$ describes the stable model while $C_s^2 < 0$ only when the model is unstable) [57, 58, 60]. The ratio of $\Omega_m = \rho_m/\rho_c$ and $\Omega_d = \rho_d/\rho_c$ called the coincidence parameter given by $\tilde{r} = \Omega_m/\Omega_d = \rho_m/\rho_d$ decides the dark energy- and dark matter-dominated eras of the universe (i.e., $0 < \Omega_m/\Omega_d < 1$ describes the dark energy-dominated era, and $\Omega_m/\Omega_d > 1$ gives the dark matter-dominated era) [61]. In the upcoming, we will discuss these cosmological parameters.

Differentiating (18) with respect to cosmic time $t$ and substituting all necessary values in it, one can get

$$\dot{H} = \frac{-3\kappa\Omega_{m_o}H_o^2\Delta a^{-\Delta} - 8\pi\kappa\omega H^2\gamma^3 a^{-2\gamma}}{48\pi\kappa - 48\pi\kappa\gamma - 8\pi\kappa\omega\gamma^2 a^{-2\gamma} - 12c^2H^2\sinh\left(\pi\kappa/H^2\right) + 6\pi\kappa c^2\cosh\left(\pi\kappa/H^2\right)}. \tag{21}$$

Using the transformation $d/dt = -(1+z)H(d/dz)$ from cosmic time $t$ to the redshift parameter $z$, simplification of (21) gives the relation for $H$ in terms of the redshift parameter as

$$H' = \frac{8\pi\kappa\omega H^2\gamma^3(1+z)^{2\gamma-1} + 3\kappa\Omega_{m_o}H_o^2\Delta(1+z)^{\Delta-1}}{H\left[48\pi\kappa - 48\pi\kappa\gamma - 8\pi\kappa\omega\gamma^2(1+z)^{2\gamma} - 12c^2H^2\sinh\left(\pi\kappa/H^2\right) + 6\pi\kappa c^2\cosh\left(\pi\kappa/H^2\right)\right]}, \tag{22}$$

where the "prime" denotes the derivative with respect to redshift parameter $z$. The deceleration parameter $q$ which is of great importance to decide the accelerated expansion of the universe can be found as

$$q = -1 - \frac{\dot{H}}{H^2} = -1 + \frac{8\pi\kappa\omega H^2\gamma^3(1+z)^{2\gamma} + 3\kappa\Omega_{m_o}H_o^2\Delta(1+z)^{\Delta}}{H^2\left[48\pi\kappa - 48\pi\kappa\gamma - 8\pi\kappa\omega\gamma^2(1+z)^{2\gamma} - 12c^2H^2\sinh\left(\pi\kappa/H^2\right) + 6\pi\kappa c^2\cosh\left(\pi\kappa/H^2\right)\right]}. \tag{23}$$

Substituting the corresponding values and simplifying (17), we obtain

$$\begin{aligned} p_d^K = \frac{3}{8\pi\kappa(\gamma-3)}\Bigg[&\left(2\pi\kappa c^2H(1+z)\cosh\left(\frac{\pi\kappa}{H^2}\right) - 4c^2H^3\right.\\ &\left.\cdot(1+z)\sinh\left(\frac{\pi\kappa}{H^2}\right)\right)H' - c^2H^4(\gamma-3)\sinh\left(\frac{\pi\kappa}{H^2}\right)\\ &+ 3\kappa b^2\Omega_{m_o}H_o^2(1+z)^{\Delta}\Bigg]. \end{aligned} \tag{24}$$

The mathematical formalism for the EoS parameter is $\omega_d^K = p_d^K/\rho_d^K$, and the relation for $\omega_d^K$ can be obtained by using (15) and (24) in this formula as

$$\begin{aligned} \omega_d^K = -1 + &\left(\frac{2\pi\kappa(1+z)\coth\left(\pi\kappa/H^2\right)}{H^3(\gamma-3)} - \frac{4(1+z)}{H(\gamma-3)}\right)H'\\ &+ \frac{3\kappa b^2\Omega_{m_o}H_o^2(1+z)^{\Delta}}{c^2H^4(\gamma-3)\sinh\left(\pi\kappa/H^2\right)}. \end{aligned} \tag{25}$$

Some other important mathematical formulas of cosmological consequences which we will use later on are

$$\begin{aligned} \Omega_m &= \frac{\rho_m}{\rho_c},\\ \Omega_d &= \frac{\rho_d}{\rho_c},\\ \frac{\Omega_m}{\Omega_d} &= \frac{\rho_m}{\rho_d},\\ \rho_c &= \frac{3H^2}{8\pi}. \end{aligned} \tag{26}$$

The ratio $\Omega_m/\Omega_d^K$ which is of great importance to decide about the dark energy- and dark matter-dominated eras of the universe for the Kaniadakis entropy content of BH is given by

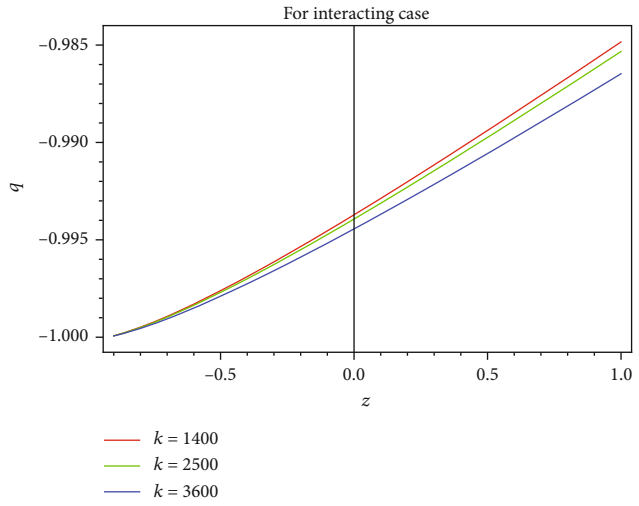


FIGURE 1: Behavior of deceleration parameter $q$ against redshift parameter $z$ considering different values of $\kappa$ when $\Omega_{m_o} = 0.315$, $b^2 = 0.5$, $H_o = 67.9$, $\omega = -0.3$, $c^2 = 0.313$, and $\gamma = 0.127$.

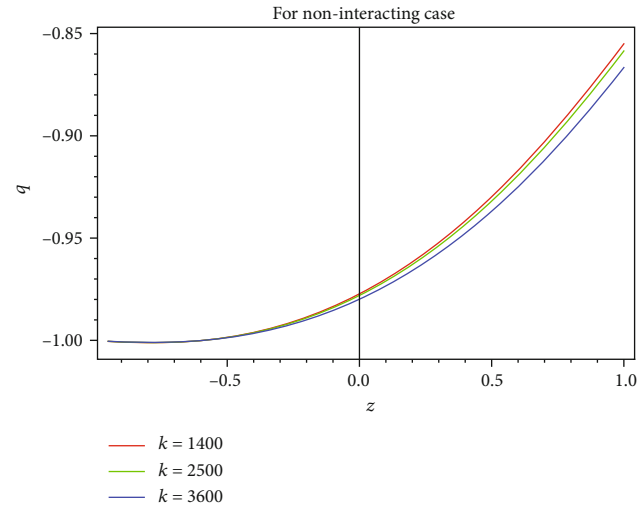


FIGURE 2: Behavior of $q$ against $z$.

$$\frac{\Omega_m}{\Omega_d^K} = \frac{\kappa\Omega_{m_o}H_o^2(1+z)^{\Delta}}{c^2H^4\sinh\left(\pi\kappa/H^2\right)}. \tag{27}$$

The stability of the system is examined by a perturbed parameter called the squared speed of sound ($C_s^2$). The mathematical formalism for this parameter is given by

$$C_s^2 = \frac{\partial p_{\text{eff}}}{\partial \rho_{\text{eff}}}, \tag{28}$$

where $\rho_{\text{eff}} = \rho_m + \rho_d^K$ and $p_{\text{eff}} = p_d^K$. Differentiating these relations with respect to the redshift parameter leads to the following mathematical result:

$$\begin{aligned} C_s^2 = {} & \frac{1}{(\gamma-3)\left[\kappa\Omega_{m_o}H_o^2\Delta(1+z)^{\Delta-1} + c^2\left[4H^3H'\sinh\left(\pi\kappa/H^2\right) - 2\pi\kappa HH'\cosh\left(\pi\kappa/H^2\right)\right]\right]} \\ & \cdot\left[2\pi\kappa c^2(1+z)\cosh\left(\frac{\pi\kappa}{H^2}\right)\left(H'^2 + HH'\times(1+z)^{-1} + HH'' + 2\pi\kappa H^{-2}H'^2\tanh\left(\frac{\pi\kappa}{H^2}\right)\right)\right. \\ & - 4(1+z)\sinh\left(\frac{\pi\kappa}{H^2}\right)c^2\left(3H^2H'^2 + H^3H'(1+z)^{-1} + H^3H'' - 2\pi\kappa\times H'^2\coth\left(\frac{\pi\kappa}{H^2}\right)\right) \\ & \left. + 3\kappa b^2\Omega_{m_o}H_o^2\Delta(1+z)^{\Delta-1} - c^2(\gamma-3)HH'\left(4H^2\sinh\left(\frac{\pi\kappa}{H^2}\right) - 2\pi\kappa\cosh\left(\frac{\pi\kappa}{H^2}\right)\right)\right]. \end{aligned} \tag{29}$$

Variation of $q$ against $z$ has been plotted for interacting (Figure 1) and noninteracting (Figure 2) cases, respectively. By considering $\kappa = 1400,2500,3600$ with fixed values of other parameters as $\Omega_{m_o} = 0.315$, $b^2 = 0.5$, $H_o = 67.9$, $\omega = -0.3$, $c^2 = 0.313$, and $\gamma = 0.127$, we obtain the cosmic acceleration phase in both cases. Also, the values of the deceleration parameter lie in the range $[-1, 0)$ which is a compatible range with observational data. In Figure 3, EoS parameter $\omega_d^K$ for the KHDE model is plotted versus deceleration parameter $q$ for the interacting case while in Figure 4, the same is plotted for the noninteracting case. The evolved constant parameters are taken, the same as in Figures 1 and 2. The phantom phase of the universe is observed for the interacting case. For the noninteracting case, the quintessence phase is achieved for $\kappa = 1400, 2500$ and the phantom phase for $\kappa = 3600$. Moreover, the EoS parameter $\omega_d^K \to -1$ as $z \to -1$ which coincides with the $\Lambda$CDM model. In Figures 5 and 6, the coincidence parameter $\tilde{r} = \Omega_m/\Omega_d^K$ is plotted against $q$ for interacting and noninteracting cases, respectively. The dark energy-dominated era is recovered for the interacting case while for the noninteracting case, when $\kappa = 1400$, the interval $-0.95 < z < 0.65$ gives the energy-dominated era while $z > 0.65$ results in the matter-dominated era; for $\kappa = 2500$, the matter-dominated era is obtained when $z > 0.83$, and for $\kappa = 3600$, the matter-dominated era is achieved when $z > 1.1$. The squared speed of sound $C_s^2$ which decides the stability of the model is examined for both cases (interacting and noninteracting) in Figures 7 and 8, respectively. For the

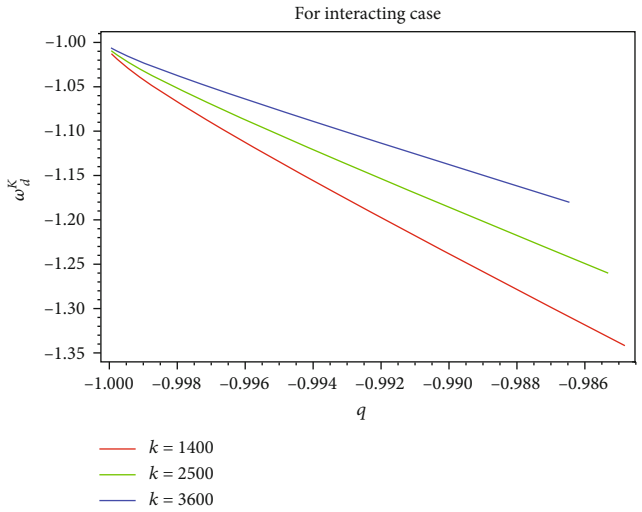


FIGURE 3: Graph of EoS $\omega_d^K$ versus deceleration parameter $q$.

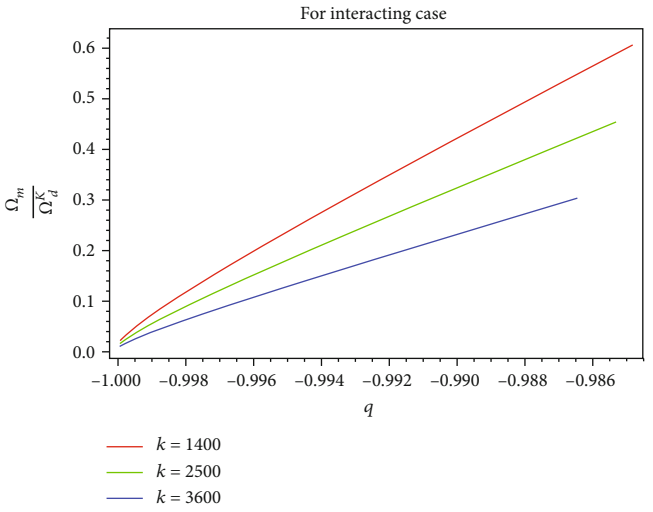


FIGURE 5: Plot of coincidence parameter $\tilde{r} = \Omega_m/\Omega_d^K$ against deceleration parameter $q$.

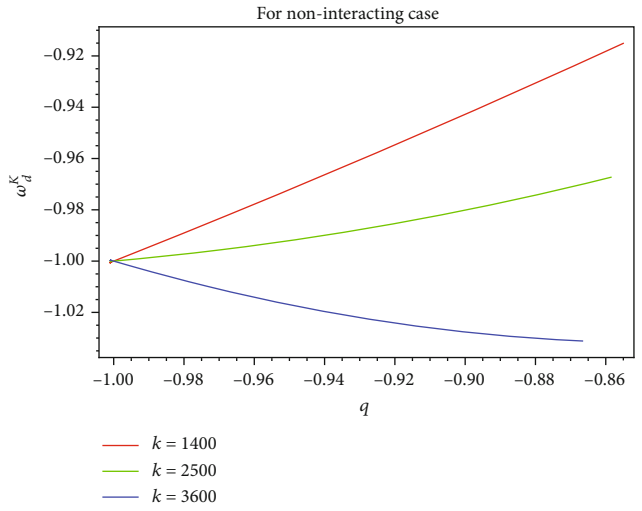


FIGURE 4: Variation of EoS parameter $\omega_d^K$ versus deceleration parameter $q$.

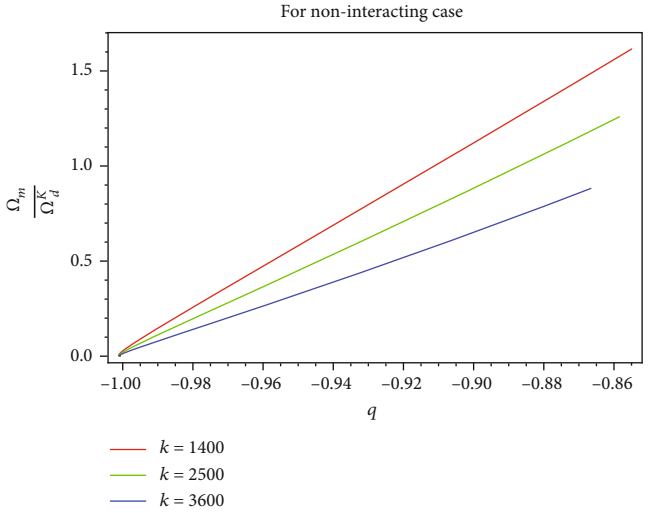


FIGURE 6: Plot of $\tilde{r} = \Omega_m/\Omega_d^K$ against $q$.

interacting case, $C_s^2 > 0$ in the interval $-0.95 < z < 0.63$ which leads to the stable model in this interval. The noninteracting case model is stable when $z < -0.18$ while it becomes unstable when $z > -0.18$.

## 4. New Tsallis Holographic Dark Energy

Considering the pattern of (14) and (15) and taking Tsallis entropy (6) into account, it is easy to have NTHDE as

$$\rho_d^T \propto \frac{S_Q^T}{L^4} \Rightarrow \rho_d^T = \left(\frac{3T^2}{8\pi}\right)\frac{S_Q^T}{L^4}, \tag{30}$$

where $T^2$ is an unknown real number [18]. Taking $D^2 = \pi T^2$ and the apparent horizon as the IR cutoff ($H = 1/L$), we have

$$\rho_d^T = \frac{2D^2\rho_c}{X}\exp\left(\frac{X}{2}\right)\sinh\left(\frac{X}{2}\right), \tag{31}$$

in which $X = \delta\pi/H^2$, where $\delta$ belongs to a set of real numbers [11]. Substituting all required assumed and obtained values in (29), we get

$$\rho_d^T = \frac{3H^4D^2}{4\pi^2\delta}\lambda, \tag{32}$$

where $\lambda = \exp(\pi\delta/2H^2)\sinh(\pi\delta/2H^2)$. Considering all assumptions, differentiating (18) w.r.t. cosmic time $t$, and putting necessary values in it, we reach the following result:

$$H' = \frac{16\pi^2\delta H\gamma^3\omega(1+z)^{2\gamma-1} + 6\pi\delta\Omega_{m_o}H_o^2\Delta(1+z)^{\Delta-1}H^{-1}}{16\pi^2\delta\left(6-6\gamma-\omega\gamma^2(1+z)^{2\gamma}\right) - 9D^2\lambda\left(16H^2 - \pi\delta\left(\coth\left(\pi\gamma/2H^2\right)+1\right)\right)}. \tag{33}$$

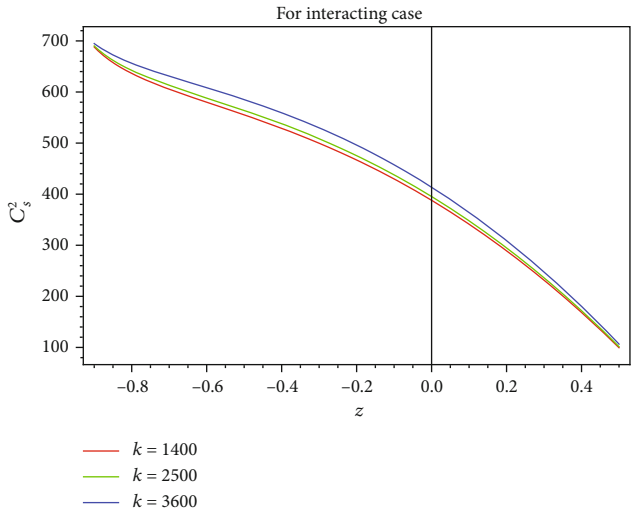


Figure 7: Variation of squared speed of sound $C_s^2$ versus redshift parameter $z$.

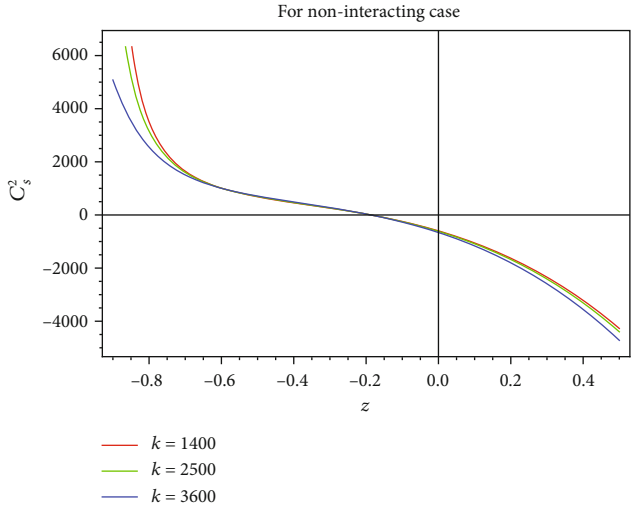


Figure 8: Variation of squared speed of sound $C_s^2$ versus redshift parameter $z$.

The deceleration parameter $q$ for the NTHDE model is obtained as

$$q = -1 - \frac{\dot{H}}{H^2} = -1 + \frac{16\pi^2\delta\gamma^3\omega(1+z)^{2\gamma} + 6\pi\delta\Omega_{m_o}H_o^2H^{-2}\Delta(1+z)^{\Delta}}{96\pi^2\delta(1-\gamma) - 16\pi^2\delta\omega\gamma^2(1+z)^{2\gamma} - 9D^2\lambda\left[16H^2 - \pi\delta\left(\coth\left(\pi\gamma/2H^2\right)+1\right)\right]}. \tag{34}$$

Substituting the concern values from the NTHDE model and simplifying Equation (17) yield

$$p_d^T = \frac{9b^2\Omega_{m_o}H_o^2(1+z)^{\Delta}}{8\pi(\gamma-3)} - \frac{3D^2H^4H'\lambda}{4\pi^2\delta} + \frac{3D^2H(1+z)\lambda H'}{4\pi(\gamma-3)} \cdot \left[\coth\left(\frac{\pi\delta}{2H^2}\right) + 1 - \frac{4H^2}{\pi\delta}\right]. \tag{35}$$

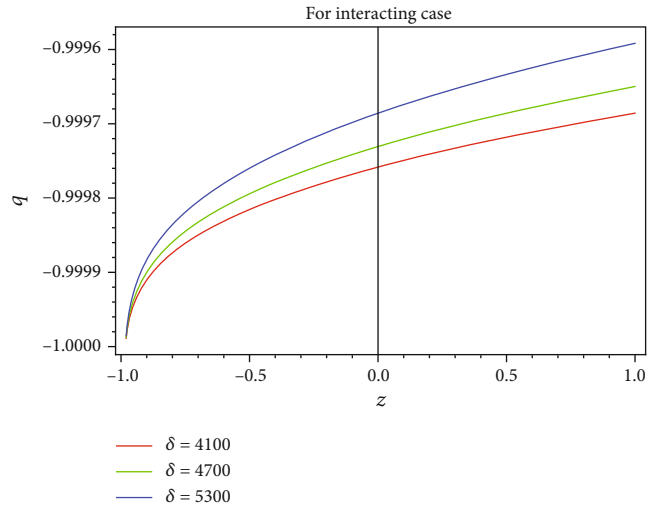


Figure 9: Variation of deceleration parameter $q$ against redshift parameter $z$ considering different values of $\delta$ when $\Omega_{m_o} = 0.315$, $b^2 = 0.5$, $\omega = -0.3$, $H_o = 67.9$, $D^2 = 0.3136$, and $\gamma = 0.127$.

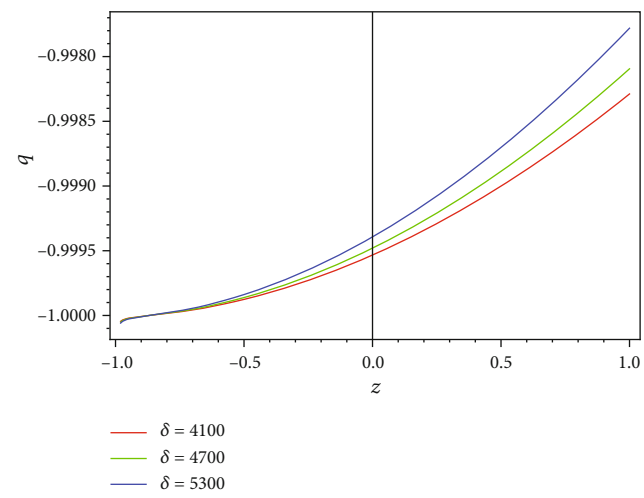


Figure 10: Graph of $q$ against $z$.

The relation for EoS parameter $\omega_d^T$ is obtainable after simplifications of Equations (32) and (35) as

$$\omega_d^T = \frac{p_d^T}{\rho_d^T} = \frac{\pi\delta b^2\Omega_{m_o}H_o^2(1+z)^{\Delta}}{2H^4D^2(\gamma-3)\lambda} - 1 + \frac{1+z}{\gamma-3} \cdot \left[\frac{\pi\delta}{4H^3}\coth\left(\frac{\pi\delta}{2H^2}\right) + \frac{\pi\delta}{4H^3} - \frac{4}{H}\right]H'. \tag{36}$$

The coincidence parameter for the obtained model is

$$\tilde{r} = \frac{\Omega_m}{\Omega_d^K} = \frac{\pi\delta\Omega_{m_o}H_o^2(1+z)^{\Delta}}{2D^2H^4\lambda}. \tag{37}$$

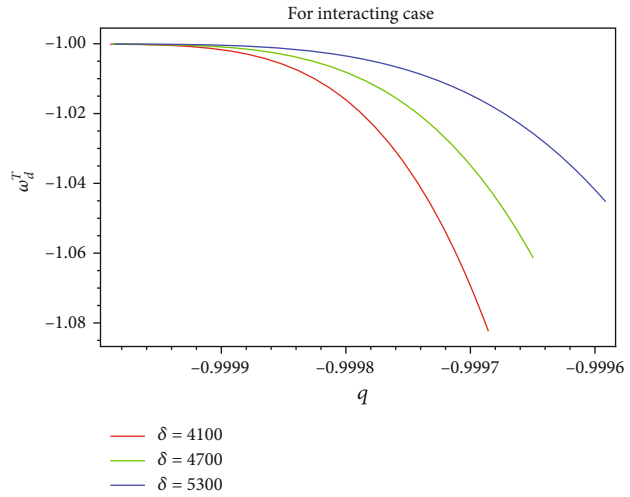


FIGURE 11: Plot of EoS parameter $\omega_d^T$ versus deceleration parameter $q$.

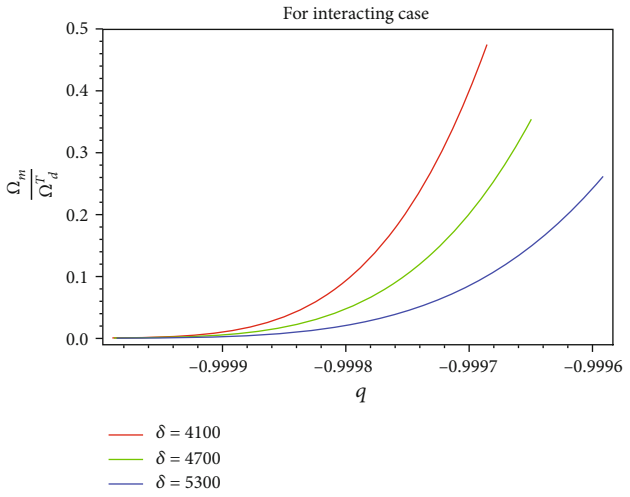


FIGURE 13: Behavior of coincidence parameter $\tilde{r} = \Omega_m/\Omega_d^T$ against deceleration parameter $q$.

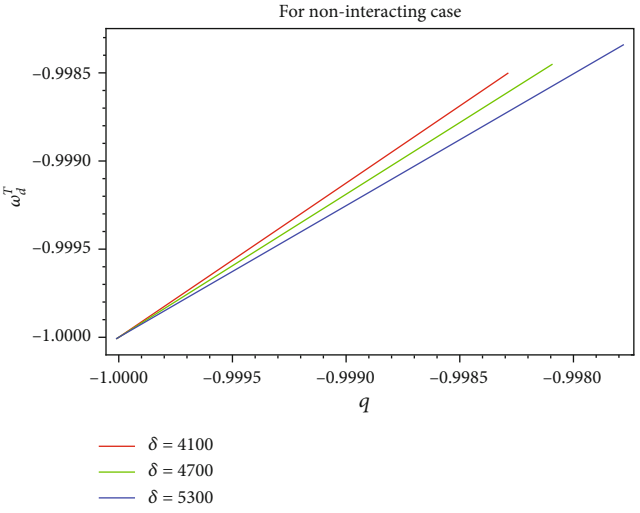


FIGURE 12: Plot of EoS parameter $\omega_d^T$ versus deceleration parameter $q$.

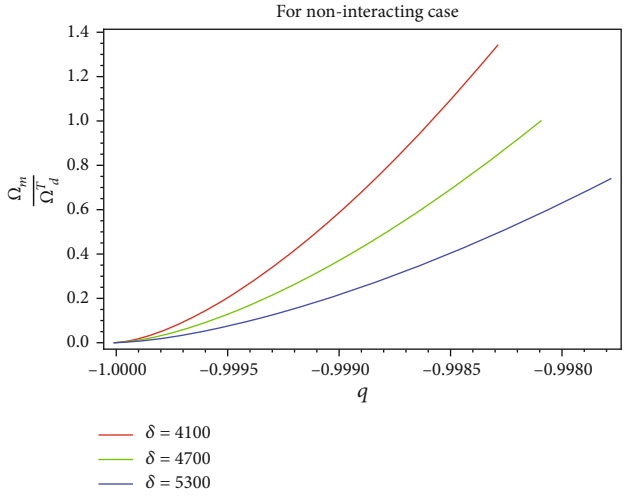


FIGURE 14: Behavior of coincidence parameter $\tilde{r} = \Omega_m/\Omega_d^T$ against $q$.

The relation for a perturbed parameter called the squared speed of sound which is given in (28) is obtainable as

$$C_s^2 = \frac{1}{(\gamma-3)\left[3\pi\delta\Omega_{m_o}H_o^2\Delta(1+z)^{\Delta-1} + 6D^2HH'\lambda\left[4H^2 - \pi\delta - \pi\delta\coth\left(\pi\delta/2H^2\right)\right]\right]}$$
$$\cdot\left[9\pi\delta b^2\Omega_{m_o}H_o^2\Delta(1+z)^{\Delta-1} + 6D^2\times(\gamma-3)HH'\lambda\right.$$
$$\cdot\left(\pi\delta\coth\left(\frac{\pi\delta}{2H^2}\right) - 4H^2 + \pi\delta\right) + 6D^2\pi\delta\beta(1+z)$$
$$\cdot\left(H'^2 + HH'(1+z)^{-1} + HH'' - \pi\delta H^{-2}H'^2 + \pi\delta\times H^{-2}H'^2\tanh\left(\frac{\pi\delta}{2H^2}\right)\right)$$
$$+ 6D^2\pi\delta(1+z)\lambda\left(H'^2 + HH'(1+z)^{-1} + HH'' - \pi\delta H^{-2}H'^2\right.$$
$$\left.\left.- \pi\delta H^{-2}H'^2\coth\left(\frac{\pi\delta}{2H^2}\right)\right) - 24D^2(1+z)\lambda\left(3H^2H'^2 + H^3H'(1+z)^{-1}\right.\right.$$
$$\left.\left.+ H^3H'' - \pi\delta H'^2 - \pi\delta H'^2\coth\left(\frac{\pi\delta}{2H^2}\right)\right)\right], \tag{38}$$

where $\beta = \exp(\pi\delta/2H^2)\cosh(\pi\delta/2H^2)$.

The graph of deceleration parameter $q$ against redshift parameter $z$ is plotted in Figures 9 and 10 for interacting and noninteracting cases, respectively. Constant parameters are $\delta = 4100,4700,5300$, $\Omega_{m_o} = 0.315$, $b^2 = 0.5$, $H_o = 67.9$, $\omega = -0.3$, $D^2 = 0.313$, and $\gamma = 0.127$. Required results (accelerated expansion) of the universe are achieved in both cases. EoS parameter $\omega_d^T$ for the NTHDE model is plotted versus deceleration parameter $q$ for interacting and noninteracting cases in Figures 11 and 12, respectively. The involved parameters are taken, the same as in Figures 9 and 10. The phantom phase of the universe is observed for the interacting case, and the quintessence phase is achieved for the noninteracting case. In Figures 13 and 14, the coincidence parameter $\tilde{r} = \Omega_m/\Omega_d^T$ is plotted against $q$ for interacting and noninteracting cases, respectively. The dark energy-dominated era is recovered for the interacting case whereas for the noninteracting case, when $\delta = 4100$, the interval $-0.95 < z < 0.8$ gives the energy-dominated era while $z > 0.8$ results in the matter-

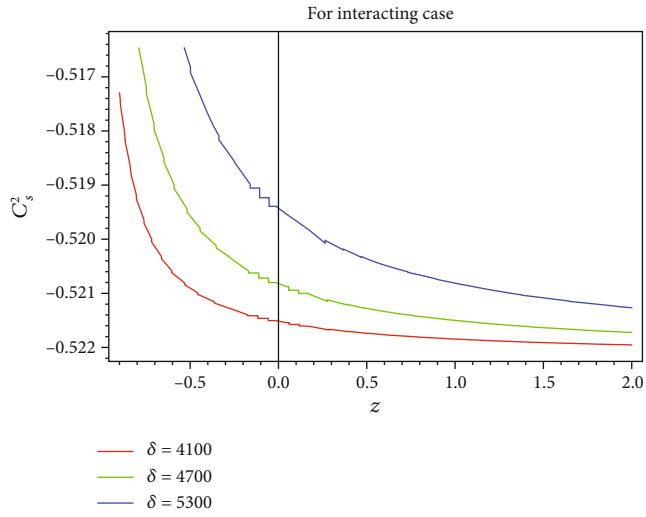


Figure 15: Plot of squared speed of sound $C_s^2$ versus redshift parameter $z$.

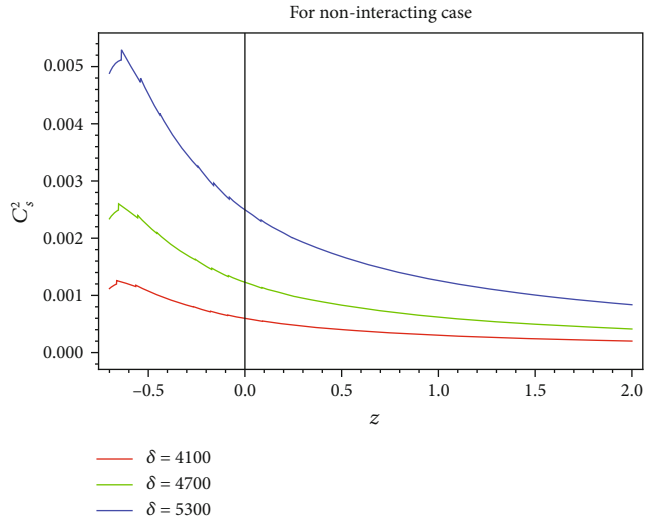


Figure 16: Graph of $C_s^2$ against $z$.

Table 1

| $q$ | Observational schemes |
|---|---|
| $-0.644^{+0.223}_{-0.223}$ | BAO+TDSL+Masers+Pantheon |
| $-0.6401^{+0.187}_{-0.187}$ | BAO+TDSL+Masers+Pantheon+$H_o$ |
| $-0.930^{+0.218}_{-0.218}$ | BAO+TDSL+Masers+Pantheon+$H_z$ |
| $-1.2037^{+0.175}_{-0.175}$ | BAO+TDSL+Masers+Pantheon+$H_o$+$H_z$ |

dominated era; for $\delta = 4700$, the matter-dominated era is obtained when $z > 1$, and for $\delta = 5300$, the matter-dominated era is achieved when $z > 1.23$. In Figures 15 and 16, the squared speed of sound $C_s^2$ has been plotted to examine the stability of the model for both the interacting and noninteracting cases, respectively. For the interacting case, $C_s^2 < 0$ while for the noninteracting case, it leads to positive values which describes the stable model.

Table 2

| $\omega_d$ | Observational schemes |
|---|---|
| $-1.56^{+0.60}_{-0.48}$ | Planck+lowE+TT |
| $-1.58^{+0.52}_{-0.41}$ | Planck+lowE+TT, TE, EE |
| $-1.57^{+0.50}_{-0.40}$ | Planck+lowE+lensing+TT, TE, EE |
| $-1.40^{+0.10}_{-0.10}$ | Planck+lowE+lensing+BAO+TT, TE, EE |

## 5. Conclusions

We have investigated the interacting and noninteracting behaviors of KHDE and NTHDE with the apparent horizon and extracted various cosmological parameters by varying the value of $\kappa$ for KHDE and $\delta$ for NTHDE and keeping all other parameters fixed as $\Omega_{m_o} = 0.315$, $b^2 = 0.5$, $H_o = 67.9$, $\omega = -0.3$, $c^2 = 0.313$, $D^2 = 0.313$, and $\gamma = 0.127$. The cosmological consequences resulted as follows.

*5.1. Deceleration Parameter.* For the KHDE model, the deceleration parameter $q$ provides the accelerated universe in both the interacting and noninteracting cases. The results obtained in both cases for $q$ are compared with Planck's observational data [62] presented in Table 1. It has been found that the results of the KHDE model are consistent with the observational data at the present epoch in both the interacting and noninteracting cases. At $z = 0$, for the interacting case, we have achieved $(\kappa, q) = (1400, -0.9937), (2500, -0.9939), (3600, -0.9944)$, and for the noninteracting case, we obtained $(\kappa, q) = (1400, -0.9773), (2500, -0.9781), (3600, -0.9800)$. The deceleration parameter $q$ has given that NTHDE can model the accelerated universe in both the interacting and noninteracting cases. The results obtained in both cases for $q$ are compared with Planck's observational data [62] presented in Table 1. It has been found that the results of the NTHDE model are consistent with the observational data at the present epoch in both the interacting and noninteracting cases. At $z = 0$, for the interacting case, we achieve $(\delta, q) = (4100, -0.99976), (4700, -0.99973), (5300, -0.99968)$, and for the noninteracting case, we obtain $(\delta, q) = (4100, -0.99954), (4700, -0.99948), (5300, -0.99939)$.

*5.2. EoS Parameter.* For the KHDE model, the EoS parameter $\omega_d^K$ has illustrated the phantom phase of the universe at different values of $\kappa$ for the interacting case. However, it shows the quintessence phase of the universe for $\kappa = 1400, 2500$ and the phantom phase for $\kappa = 3600$ when the noninteracting case is under consideration. Moreover, we compared these results with Planck's observational data [62] presented in Table 2. The comparison shows that results obtained by the KHDE model have consistency with the observational data at $z = 0$ in both cases. For the interacting case, we found the values of $(\kappa, \omega_d^K)$ at the present epoch as $(1400, -1.16), (2500, -1.12), (3600, -1.08)$ while for the noninteracting case, we achieve $(\kappa, \omega_d^K) = (1400, -0.988), (2500, -0.997), (3600, -1.007)$. For the NTHDE model, the EoS parameter $\omega_d^T$ tells about the phantom phase of the universe at different values of $\delta$ for the interacting case while it shows the quintessence

phase of the universe for the noninteracting case. Moreover, we compared these results obtained with Planck's observational data [62] presented in Table 2. The comparison shows that results obtained by the NTHDE model have consistency with the observational data at $z = 0$ in both cases. For the interacting case, we found the values of $(\delta, \omega_d^T)$ at the present epoch as $(4100,-1.032), (4700,-1.023), (5300,-1.017)$, and for the noninteracting case, we achieve $(\delta, \omega_d^T) = (4100,-0.99959), (4700,-0.99958), (5300,-0.99955)$.

*5.3. Coincidence Parameter.* For the KHDE model, the coincidence parameter $\tilde{r} = \Omega_m/\Omega_d^K$ is achieved for both the interacting and noninteracting cases. For the interacting case, we obtain the dark energy-dominated era for $-0.95 < z < 1$. For the noninteracting case, when $\kappa = 1400$, the interval $-0.95 < z < 0.65$ gives the energy-dominated era while $z > 0.65$ results in the matter-dominated era; for $\kappa = 2500$, the matter-dominated era is obtained when $z > 0.83$, and for $\kappa = 3600$, the matter-dominated era is achieved when $z > 1.1$. The coincidence parameter for the NTHDE model $\tilde{r} = \Omega_m/\Omega_d^K$ has been examined for both the interacting and noninteracting cases. For the interacting case, we got the dark energy-dominated era in the interval $-0.95 < z < 1$. For the noninteracting case, when $\delta = 4100$, the interval $-0.95 < z < 0.8$ gives the energy-dominated era while $z > 0.8$ results in the matter-dominated era; for $\delta = 4700$, the matter-dominated era is obtained when $z > 1$, and for $\delta = 5300$, the matter-dominated era is achieved when $z > 1.23$.

*5.4. Squared Speed of Sound.* The squared speed of sound $C_s^2$ which decides the stability of the model is examined for both the interacting and noninteracting cases. For the interacting case, $C_s^2 > 0$ in the interval $-0.95 < z < 0.63$ which is a justification for the stable model in this interval while the KHDE model is unstable when $z > 0.63$. For the noninteracting case model, behavior is stable when $z < -0.1873$ while it becomes unstable when $z > -0.1873$. For the NTHDE model, the squared speed of sound $C_s^2$ is examined for both the interacting and noninteracting cases. For the interacting case, $C_s^2 < 0$ which gives that the achieved model is unstable for the interacting case but it has given positive values of $C_s^2$ for the noninteracting case in the interval $-0.95 < z < 2$, which is a justification for the stable model.

Ghaffari et al. investigated the cosmological consequences of the interacting THDE model with the apparent radius in the fractal universe [36]. They constructed various cosmological parameters such as the EoS parameter, the deceleration parameter, and the evolution equation. They suggested that THDE described the transition that took place from the deceleration phase of the universe to the accelerated phase, eventually in both the noninteracting and interacting scenarios. Also, it is checked that the free parameters of the models are compatible with the latest observational results by using the Pantheon supernovae data, 6df, eBOSS, BOSS DR12, CMB Planck 2015, and Gamma-Ray Burst. They also found unstable behavior of the THDE model in both scenarios. However, in our case, KHDE and NTHDE with the apparent horizon in the fractal universe have provided consistent results with recent Planck's data [37] (as mentioned in Tables 1 and 2). It is also found that at the present epoch, the KHDE model is stable for the interacting case but unstable for the noninteracting case. The NTHDE model shows unstable behavior for the interacting case while stable behavior for the noninteracting case.

## Data Availability

I have mentioned all the results in the manuscript and references therein.

## Conflicts of Interest

The authors declare that they have no conflicts of interest.

## References

[1] J. W. Gibbs, *Elementry Priciples in Statistical Mechanics*, Charles Scribner's Sons, New York, 1902.

[2] G. Kaniadakis, "Non-linear kinetics underlying generalized statistics," *Physica A: Statistical Mechanics and its Applications*, vol. 296, no. 3-4, pp. 405–425, 2001.

[3] G. Kaniadakis, "Statistical mechanics in the context of special relativity," *Physical Review E*, vol. 66, no. 5, 2002.

[4] M. Masi, "A step beyond Tsallis and Renyi entropies," *Physics Letters A*, vol. 338, no. 3-5, pp. 217–224, 2005.

[5] N. Komatsu, "Cosmological model from the holographic equipartition law with a modified Rényi entropy," *The European Physical Journal C*, vol. 77, no. 4, 2017.

[6] H. Moradpour, A. Bonilla, E. M. . C. Abreu, and J. A. Neto, "Accelerated cosmos in a nonextensive setup," *Physical Review D*, vol. 96, no. 12, 2017.

[7] E. M. C. Abreu, J. A. Neto, A. C. R. Mendes, A. Bonilla, and R. M. de Paula, "Tsallis' entropy, modified Newtonian accelerations and the Tully-Fisher relation," *EPL (Europhysics Letters)*, vol. 124, no. 3, p. 30005, 2018.

[8] A. Bialas and W. Czyz, "Renyi entropies of a black hole from Hawking radiation," *EPL (Europhysics Letters)*, vol. 83, no. 6, p. 60009, 2008.

[9] V. G. Czinner and H. Iguchi, "Thermodynamics, stability and Hawking–Page transition of Kerr black holes from Rényi statistics," *The European Physical Journal C*, vol. 77, no. 12, 2017.

[10] J. Sadeghi, M. Rostami, and M. R. Alipour, "Investigation of phase transition of BTZ black hole with Sharma–Mittal entropy approaches," *International Journal of Modern Physics A*, vol. 34, no. 30, p. 1950182, 2019.

[11] H. Moradpour, A. H. Ziaie, and M. K. Zangeneh, "Generalized entropies and corresponding holographic dark energy models," *The European Physical Journal C*, vol. 80, no. 8, 2020.

[12] M. Tavayef, A. Sheykhi, K. Bamba, and H. Moradpour, "Tsallis holographic dark energy," *Physics Letters B*, vol. 781, pp. 195–200, 2018.

[13] H. Moradpour, S. A. Moosavi, I. P. Lobo, J. P. M. Graça, A. Jawad, and I. G. Salako, "Thermodynamic approach to holographic dark energy and the Rényi entropy," *The European Physical Journal C*, vol. 78, no. 10, 2018.

[14] H. Moradpour, A. H. Ziaie, S. Ghaffari, and F. Feleppa, "The generalized and extended uncertainty principles and their implications on the Jeans mass," *Monthly Notices of the Royal Astronomical Society*, vol. 488, no. 1, pp. L69–L74, 2019.

[15] H. Moradpour, A. Sheykhi, C. Corda, and I. G. Salako, "Implications of the generalized entropy formalisms on the Newtonian gravity and dynamics," *Physics Letters B*, vol. 783, pp. 82–85, 2018.

[16] J. D. Barrow, "The area of a rough black hole," *Physics Letters B*, vol. 808, no. 135643, article 135643, 2020.

[17] S. Ghaffari, A. H. Ziaie, V. B. Bezerra, and H. Moradpour, "Inflation in the Rényi cosmology," *Modern Physics Letters A*, vol. 35, no. 1, article 1950341, 2020.

[18] M. Li, "A model of holographic dark energy," *Physics Letters B*, vol. 603, no. 1-2, pp. 1–5, 2004.

[19] M. Srednicki, "Entropy and area," *Physical Review Letters*, vol. 71, no. 5, pp. 666–669, 1993.

[20] S. Das and S. Shankaranarayanan, "Where are the black-hole entropy degrees of freedom?," *Classical and Quantum Gravity*, vol. 24, no. 20, pp. 5299–5306, 2007.

[21] D. Pavon, "On the degrees of freedom of a black hole," 2020, https://arxiv.org/abs/2001.05716.

[22] S. A. Hayward, "Unified first law of black-hole dynamics and relativistic thermodynamics," *Classical and Quantum Gravity*, vol. 15, no. 10, pp. 3147–3162, 1998.

[23] D. Bak and S.-J. Rey, "Cosmic holography+," *Classical and Quantum Gravity*, vol. 17, no. 15, pp. L83–L89, 2000.

[24] R.-G. Cai and S. P. Kim, "First law of thermodynamics and Friedmann equations of Friedmann–Robertson–Walker universe," *Journal of High Energy Physics*, vol. 2005, no. 2, pp. 50–50, 2005.

[25] M. Akbar and R.-G. Cai, "Thermodynamic behavior of the Friedmann equation at the apparent horizon of the FRW universe," *Physical Review D*, vol. 75, no. 8, 2007.

[26] Y. S. Myung, "Instability of holographic dark energy models," *Physics Letters B*, vol. 652, no. 5-6, pp. 223–227, 2007.

[27] Q. Huang, H. Huang, J. Chen, L. Zhang, and F. Tu, "Stability analysis of a Tsallis holographic dark energy model," *Classical and Quantum Gravity*, vol. 36, no. 17, p. 175001, 2019.

[28] C. Tsallis, "Possible generalization of Boltzmann-Gibbs statistics," *Journal of Statistical Physics*, vol. 52, no. 1-2, pp. 479–487, 1988.

[29] A. Cho, "Statistical physics: a fresh take on disorder, or disorderly science," *Science*, vol. 297, no. 5585, pp. 1268-1269, 2002.

[30] S. Pressé, K. Ghosh, J. Lee, and K. A. Dill, "Nonadditive entropies yield probability distributions with biases not warranted by the data," *Physical Review Letters*, vol. 111, no. 18, p. 180604, 2013.

[31] V. C. Dubey, U. K. Sharma, and A. Beesham, "Tsallis holographic model of dark energy: cosmic behavior, statefinder analysis and $\omega_D - \omega_D'$ pair in the nonflat universe," *International Journal of Modern Physics D*, vol. 28, no. 15, p. 1950164, 2019.

[32] U. K. Sharma and V. C. Dubey, "Rényi holographic dark energy in the Brans–Dicke cosmology," *Modern Physics Letters A*, vol. 35, no. 34, p. 2050281, 2020.

[33] U. K. Sharma and S. Srivastava, "The cosmological behavior and the statefinder diagnosis for the new Tsallis agegraphic dark energy," *Modern Physics Letters A*, vol. 35, no. 38, p. 2050318, 2020.

[34] U. K. Sharma and V. Srivastava, "Tsallis HDE with an IR cutoff as Ricci horizon in a flat FLRW universe," *New Astronomy*, vol. 84, p. 101519, 2021.

[35] S. Srivastava and U. K. Sharma, "Barrow holographic dark energy with Hubble horizon as IR cutoff," *International Journal of Geometric Methods in Modern Physics*, vol. 18, no. 1, p. 2150014, 2021.

[36] S. Ghaffari, E. Sadri, and A. H. Ziaie, "Tsallis holographic dark energy in fractal universe," *Modern Physics Letters A*, vol. 35, no. 14, p. 2050107, 2020.

[37] P. A. Ade, N. Aghanim, M. Arnaud et al., "Planck 2015 results-XVIII. Background geometry and topology of the universe," *Astronomy & Astrophysics*, vol. 594, p. A13, 2016.

[38] R. C. Nunes, E. M. B. Jr, E. M. C. Abreu, and J. A. Neto, "Probing the cosmological viability of non-Gaussian statistics," *Journal of Cosmology and Astroparticle Physics*, vol. 2016, no. 8, pp. 51–51, 2016.

[39] M. Nauenberg, "Critique of q-entropy for thermal statistics," *Physical Review E*, vol. 67, no. 3, 2003.

[40] G. A. Tsekouras, A. Provata, and C. Tsallis, "Nonextensivity of the cyclic lattice Lotka-Volterra model," *Physical Review E*, vol. 69, no. 1, 2004.

[41] W. Li, Q. A. Wang, L. Nivanen, and A. le Méhauté, "On different q-systems in nonextensive thermostatistics," *The European Physical Journal B*, vol. 48, no. 1, pp. 95–100, 2005.

[42] S. Abe, "Temperature of nonextensive systems: Tsallis entropy as Clausius entropy," *Physica A: Statistical Mechanics and its Applications*, vol. 368, no. 2, pp. 430–434, 2006.

[43] T. S. Biro and P. Van, "Publisher's note: zeroth law compatibility of nonadditive thermodynamics," *Physical Review E*, vol. 84, no. 1, 2011.

[44] N. Farvardin and F. Y. Lin, "Performance of entropy-constrained block transform quantizers," *IEEE Transactions on Information Theory*, vol. 37, no. 5, pp. 1433–1439, 1991.

[45] E. T. Jaynes, "Gibbs vs Boltzmann entropies," *American Journal of Physics*, vol. 33, no. 5, pp. 391–398, 1965.

[46] H. Moradpour, C. Corda, A. H. Ziaie, and S. Ghaffari, "The extended uncertainty principle inspires the Rényi entropy," *EPL (Europhysics Letters)*, vol. 127, no. 6, p. 60006, 2019.

[47] K. Mejrhit and S.-E. Ennadifi, "Thermodynamics, stability and Hawking-Page transition of black holes from non- extensive statistical mechanics in quantum geometry," *Physics Letters B*, vol. 794, pp. 45–49, 2019.

[48] A. Sayahian Jahromi, S. A. Moosavi, H. Moradpour et al., "Generalized entropy formalism and a new holographic dark energy model," *Physics Letters B*, vol. 780, pp. 21–24, 2018.

[49] L. Amendola, "Scaling solutions in general nonminimal coupling theories," *Physical Review D*, vol. 60, no. 4, 1999.

[50] L. Amendola, "Coupled quintessence," *Physical Review D*, vol. 62, no. 4, 2000.

[51] B. Wang, Y. Gong, and E. Abdalla, "Transition of the dark energy equation of state in an interacting holographic dark energy model," *Physics Letters B*, vol. 624, no. 3-4, pp. 141–146, 2005.

[52] Z. K. Guo, N. Ohta, and S. Tsujikawa, "Probing the coupling between dark components of the universe," *Physical Review D*, vol. 76, p. 023508, 2007.

[53] M. Khurshudyan and R. Myrzakulov, "Phase space analysis of some interacting Chaplygin gas models," *European Physical Journal C: Particles and Fields*, vol. 77, no. 2, p. 65, 2017.

[54] E. Sadri, M. Khurshudyan, and D. F. Zeng, "Scrutinizing various phenomenological interactions in the context of holographic Ricci dark energy models," *European Physical Journal C: Particles and Fields*, vol. 80, no. 5, p. 393, 2020.

[55] A. Jawad, S. Butt, S. Rani, and K. Asif, "Cosmological aspects of sound speed parameterizations in fractal universe," *The European Physical Journal C*, vol. 79, no. 11, p. 926, 2019.

[56] V. K. Oikonomou, 2020, https://arxiv.org/abs/2012.000586v1.

[57] S. Ali, S. Khan, and S. Sattar, 2020, https://arxiv.org/abs/2011.10046v1.

[58] A. A. Mamon, A. H. Ziaie, and K. Bamba, "A generalized interacting Tsallis holographic dark energy model and its thermodynamic implications," *European Physical Journal C: Particles and Fields*, vol. 80, no. 10, p. 974, 2020.

[59] A. Jawad, Z. Khan, and S. Rani, "Cosmological and thermodynamics analysis in Weyl gravity," *The European Physical Journal C*, vol. 80, no. 1, p. 71, 2020.

[60] U. Debnath, "Constructions of $f(R, G, \mathcal{T})$ gravity from some expansions of the universe," *International Journal of Modern Physics A*, vol. 35, no. 31, p. 2050203, 2020.

[61] A. Jawad, S. Rani, S. Saleem, K. Bamba, and R. Jabeen, "Cosmological consequences of a parametrized equation of state," *Symmetry*, vol. 11, no. 8, p. 1009, 2019.

[62] N. Aghanim, Y. Akrami, M. Ashdown et al., "Planck 2018 results-VI. Cosmological parameters," *Astronomy and Astrophysics*, vol. 641, p. A6, 2020.